Composite Structures 337 (2024) 118066

Contents lists available at ScienceDirect

Composite Structures

journal homepage: www.elsevier.com/locate/compstruct

An evaluation of large diameter through-thickness metallic pins in composites

Geoffrey Neale [a,*], Vinodhen Saaran [a], Monali Dahale [b], Alex Skordos [a]

[a] Composites and Advanced Materials Centre, School of Aerospace, Transport and Manufacturing, Cranfield University, Wharley End, Bedford MK43 0AL, UK
[b] Engineering Research Institute, Ulster University, Belfast Campus, Belfast BT15 1ED, UK

ARTICLE INFO

Keywords:
Through-thickness reinforcement
Carbon fibre
Benzoxazine
Damage mechanics
Finite element analysis (FEA)

ABSTRACT

There is increasing demand for functional through-thickness reinforcement (TTR) in composites using elements whose geometry exceeds limitations of existing TTR methods like tufting, stitching, and z-pinning. Recently, static insertion of large diameter TTR pins into heated prepreg stacks has proven a feasible and robust reinforcement process capable of providing accurate TTR element placement with low insertion forces and lower tow damage compared with existing methods for similar element sizes (>1mm diameter) like post-cure drilling. Local mechanical performance and failure mechanics of these pinned laminates are reported here. Laminates with a single statically inserted pins (1.2, 1.5, and 2.0 mm) can mostly retain their in-plane integrity alongside a local improvement in mode I delamination toughness in carbon fibre-benzoxazine laminates. Tensile strength is mostly unaffected by the pins resulting from delamination suppression, whereas there is up to a doubling of Young's modulus. Compressive strength is significantly diminished (up to 42 %) in pinned laminates. Interlaminar toughness is improved, and peak toughness is pushed ahead of the crack as pin diameter increases. The lack of significant deterioration in in-plane tensile properties in pinned laminates produced using static insertion can expand the range and forms of materials that can be inserted compared to existing TTR.

1. Introduction

Recent developments in composite industry trends and growing demand are seeing functional through-thickness reinforcement (TTR) in composites become an expanding area of research interest [1]. Although TTR in composites is primarily used to improve delamination resistance [2,3], it is suited to the integration of functional elements, e.g., for thermal/electrical management [4–7], sensing [8] and joining functionalities [9–11]. Previous work on the static insertion of large diameter TTR pins into heated prepreg stacks [12] has proven that it is a feasible and robust reinforcement process. The process can provide accurate TTR element placement with low insertion forces and less fibre damage compared with existing methods for similar element sizes (>1 mm diameter), like post-cure drilling [13], and far exceeds the limitations of existing TTR methods in terms of reinforcement geometry and stiffness [14,15]. Static insertion has been developed specifically for the embedding of singular photonic sensors [16] in composite tooling, but has wider immediate implications for joining applications, and the more efficient integration of moulded-in holes. Rather than focusing on an array of sub-millimetre pins, the novelty here focuses on inserting a single, large reinforcing pin into composite comparable components that would typically require drilling e.g., bolts and fluid flow channels. The research gap here is that the local mechanical performance and failure mechanics of these laminates with single embedded pins has not been reported and analysed.

Few studies have investigated the mechanical response of woven laminates with large pins, most instead focusing on a comparison of filled- or open-hole moulded-in holes with drilled holes. Kumar et al. [17] compared 4 mm diameter open-hole and filled-hole tensile performance in moulded-in and drilled jute-epoxy/-polyester composite laminates. The quality, and by extension, the performance of specimens with moulded-in holes is significantly better than those with drilled holes, about a 28–77 % better tensile failure strength depending on specimen diameter to width (d/w) ratio, with strength comparable to virgin laminate [17]. The findings of Zitoune et al. [18] in unidirectional (UD) quasi-isotropic laminates and Langella et al. [19] in woven laminates support that of Kumar et al. [17], with the added observation that the maximum tensile stresses in filled moulded-in hole specimens decrease as hole diameter increases, but independently of d/w ratio. In UD quasi-isotropic z-pinned laminates, both tensile strength and

* Corresponding author.
E-mail address: g.d.neale@cranfield.ac.uk (G. Neale).

https://doi.org/10.1016/j.compstruct.2024.118066
Received 9 October 2023; Received in revised form 6 February 2024; Accepted 21 March 2024
Available online 24 March 2024

modulus decrease with increasing pin density, resulting from local fibre breakage and large resin rich regions. However, this is not a fair comparison because the lack of transverse plies does not constrain fibre deformation and hence resin region formation.

In compression, most studies on pin reinforcement of large diameter (>1 mm) focus on bolted [13,20] or moulded-in holes [21]. In z-pinned laminates with 0.28 mm and 0.51 mm diameter pins, compression strength decreases by ~13 % with increasing pin diameter [22] which is attributed to increased fibre waviness that results in tow kinking and subsequent bucking during failure. The consensus amongst researchers is that the presence of the opening, either filled or unfilled, results in significant changes to macroscale failure mechanisms in both tension [17,19,23–25] and compression [26,27]. Large diameter pins are virtually unexplored in the realm of mode I delamination resistance. Similar comparisons can be made to that of the single pin response (sub-millimetre) in z-pinned laminates, which is known to have positive effects on mode I the delamination resistance [28,29], with very few examples of > 1 mm diameter TT rods/pins evaluated in mode II [30].

This work evaluates the implications of using the previously reported static insertion method [12] for integrating single large diameter pins on the mechanical performance of carbon-benzoxazine laminates. This is achieved through characterising the mechanical properties and associated failure damage mechanisms in laminates with a single statically inserted pin subjected to in-plane (tension and compression) and out-of-plane (interlaminar mode I) loading conditions. The work compares failure in unpinned and pinned laminates and goes on to investigate the effect of increasing pin diameter (1.2, 1.5, and 2.0 mm) on failure progression. Links between pin insertion quality and its effect on failure progression are also explored. An experimentally validated double cantilever beam (DCB) macroscale delamination finite element model is developed to investigate the effect of pin diameter on delamination toughness.

The novelty of this work is in demonstrating that single large diameter (>1 mm) pins can be embedded in composites without adverse effects on the crucial tensile properties and a marked improvement in delamination resistance. The research contributes to addressing the demand for TTR methods capable of integrating larger functional elements, not possible with existing TTR methods, and will have significant impact by supporting the drive towards embedding multi-functionality in composites alongside positive implications for sustainability through repair and recycling.

2. Methodology

2.1. Materials and manufacturing

The material system used in this work was 12 k (650 gsm) BX180-220 carbon-benzoxazine prepreg manufactured by SHD Composite Materials Ltd. [31]. The prepreg has a 2 × 2 twill weave architecture with each cured ply of this material measuring ~0.66 mm in thickness with a fibre volume fraction (v_f) of ~60 %. The properties of the prepreg used in this study are highly desirable because the material is semi-rigid at room temperature [31,32], meaning that post-insertion cooling to room temperature fixes the through-thickness (TT) pins in place. The recommended cure cycle for this material is 2 h at 160 °C followed by 2 h at 180 °C under 6 bar autoclave pressure.

Metal TT pins were manufactured from 304L stainless steel [33] rods with diameters of 1.2, 1.5 and 2.0 mm machined to a length of 25 mm for pin insertion with the embedded pins further machined to the cured composite thickness. A 45° conical point was machined into the leading edge of the rods to allow for parting of the prepreg tows in the preform during the insertion process (Fig. 1a).

2.2. Pin insertion

Pin insertion was carried out using a TA.HDplus Texture Analyser [34], which is a universal testing machine with a 1 kN load cell, a force resolution of 1 N and a displacement resolution of 0.001 mm. Fig. 1a and c show the experimental setup of the insertion apparatus comprising the TA.HDplus Texture Analyser with a hot plate placed on the lower platen and a stainless-steel pin holder tightened between the upper grips. These pin holders were 25 mm × 25 mm × 25 mm stainless steel cubes with a 4 mm deep hole (corresponding to the various pin sizes) machined into one of its faces. Stainless-steel pin insertion fixtures for single-pin (Fig. 1b) and multi-pin (Fig. 1c) insertion were designed to guide the positioning of the pins during insertion. The multi-pin insertion fixture facilitated a row of 5 insertion points with 20 mm between each pin for a maximum prepreg stack of dimension 300 mm × 150 mm × 15 mm.

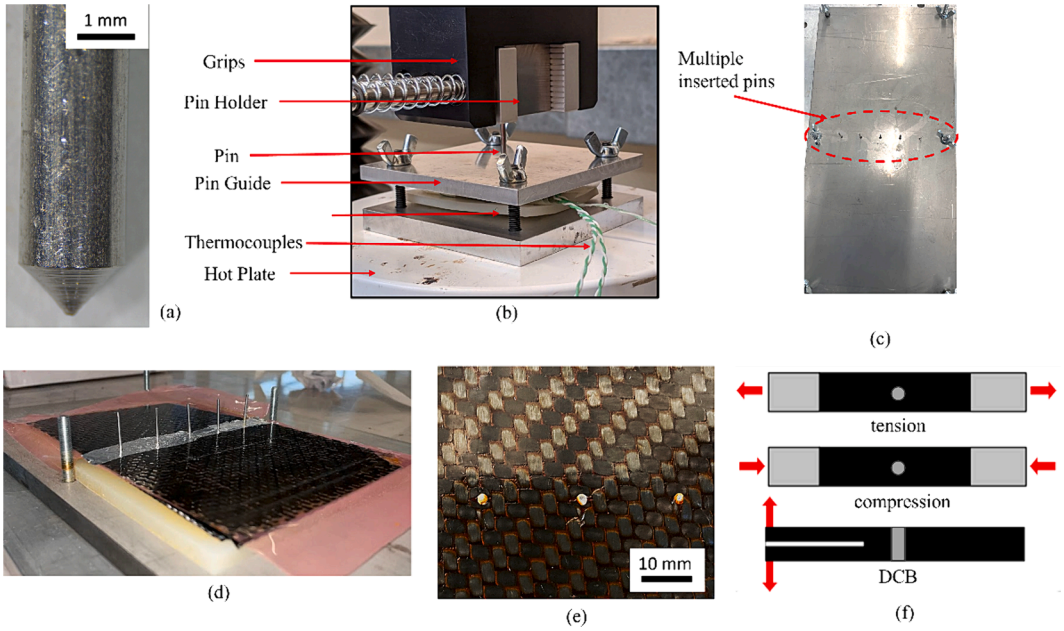

Fig. 1. Experimental setup for pin insertion showing (a) pin leading edge geometry [12], (b) single pin insertion set-up [12], (c) multi-pin insertion jig, (d) insertion-length pins embedding in prepreg stack, (e) pins embedded in cured composite, and (f) specimen configuration showing pin location.

The method for the static insertion of large-diameter metallic pins into heated woven prepreg stacks is fully characterised in a previous work [12]. Prepreg stacks of 300 mm × 150 mm were cut and laid-up according to the configurations: tension - $[0/90F,\pm45F]_s$, compression - $[0/90F,\pm45F]_s$, and double cantilever beam (DCB) - $[0/90F]_{3s}$, then consolidated on a vacuum table at 35 °C for 20 min. In the case of DCB samples a 75 mm × 170 mm sheet of Teflon film was inserted at the midplane of the stack during layup. Preforms were then placed in the multi-pin insertion fixture on a 300 mm × 150 mm × 5 mm square of 50 Shore hardness silicone. This silicone backing layer was placed between the prepreg stack and the base plate to allow for pin penetration past the bottom prepreg layer. A layer of release film was then placed over the top prepreg layer except for the strip along which pins would be inserted. This strip was covered with a layer of aluminium foil, which was far easier for the pins to penetrate without dragging the release film downwards through the stack, while still providing a barrier between the top plate of the fixture and the liquid resin upon heating for insertion. K-type thermocouples were placed between the top surface of the backing silicone and the bottom layer of the preform and between the top layer of the preform and the top plate of the insertion fixture (Fig. 1b).

The insertion fixture assembly was then clamped shut and placed into an oven at 90 °C until all the thermocouples registered a suitable insertion temperature between 60 and 80 °C (about 30–45 min) [12]. The insertion fixture assembly was then transferred to the hot plate which was maintained at 60 °C. Pins were placed into the guide plate holes and the top grip with the pin holder was then lowered to contact the back end of the pin. Once the pin alignment and preform stack temperatures were verified, the insertion was carried out at a fixed displacement rate of 0.5 mm/s until penetration of the silicone backing layer. Once insertion was completed, the upper grip was raised, leaving the pin lodged in the prepreg stack (Fig. 1d).

2.3. Curing and specimen preparation

After insertion and cooling to room temperature, the preform was removed from the insertion fixture and the inserted pins were removed by hand (pull-out) and immediately replaced with flat-edged pins of the same diameter but machined to match the composite thickness. This is done while the stack is still a preform (before curing) and done very quickly to avoid potential hole shrinkage, but in practice the substitute flat-edged pins slide in easily with no visible damage. Heating during pin insertion does not significantly affect the resin cure state [12] but resin flow under consolidation pressure more deeply impregnates the fibres. This combined with the semi-rigid nature of benzoxazine resin (BX180-220) at room temperature, perfectly preserves the geometry of the hole and allows for virtually damage free substitution of the pins. This pin replacement is necessary because the full-length through-thickness rods have a conical leading edge (to facilitate insertion) which would affect a flat surface finish, are too thick to cut cleanly by hand while embedded in the preform, and the exposed length would need significant stabilisation for autoclave curing and risks penetrating the vacuum bag.

This was cured according to the manufacturer's instructions in an autoclave for 2 h at 160 °C followed by 2 h at 180 °C under 6 bar pressure [31]. The result is shown in Fig. 1e. After curing, mechanical testing specimens were cut from the composite plates with specifications according to Table 1 and Fig. 1f.

2.4. Mechanical testing

Tension tests were carried out on an Instron 5500R universal testing machine with a 30 kN load cell. Specimens were manufactured according to Table 1 with a single pin located at each specimen centre point and with 60 mm long aluminium gripping tabs bonded to both faces at either end in accordance with ASTM D3039 [35] for unpinned and ASTM D6742 [36] for pinned specimens. Testing was carried out at a constant crosshead displacement rate of 2 mm/min.

Table 1
Mechanical testing sample configurations.

Sample	No. of specimens	Pin diameter (mm)	Specimen dimensions [l × w × h] (mm)	Test Standard
Tension	5	unpinned	250 × 25 × 2.64	ASTM D3039 [35]
		ø1.2	200 × 7.2 × 2.64	ASTM D6742 [36]
		ø1.5	200 × 9 × 2.64	$\frac{w}{d_{pin}} = 6$*
		ø2.0	200 × 12 × 2.64	
Compression	5	unpinned	80 × 12.4 × 2.64	Boeing-modified ASTM D695 [37]
		ø1.2	80 × 7.2 × 2.64	Boeing-modified ASTM D6742 [36]
		ø1.5	80 × 9 × 2.64	$\frac{w}{d_{pin}} = 6$*
		ø2.0	80 × 12 × 2.64	
Double Cantilever Beam (DCB)	5	unpinned	125 × 20 × 3.96	BS:ISO 15,024 [38]
		ø1.2	125 × 20 × 3.96	
		ø1.5	125 × 20 × 3.96	
		ø2.0	125 × 20 × 3.96	

* w/d_{pin} = width to pin diameter ratio with each specimen having a single in at its centre.

Compression tests were also carried out on an Instron 5500R universal testing machine with a 100 kN load cell and anti-buckling fixture. Specimens were manufactured according to Table 1 with a single pin located at each specimen centre point. Stainless-steel tabs with a length of 37.6 mm were bonded onto both faces at either end, leaving only a 4.8 mm open gauge length in accordance with the Boeing-modified versions of ASTM D695 [37] and ASTM D6742 [36]. Specimens were tested with a constant crosshead displacement of 1 mm/min.

Double cantilever beam testing was carried out on a Zwick Z010 universal testing machine with a 2 kN load cell. Specimens were manufactured according to Table 1 and tested according to BS:ISO 15024 [38]. A Teflon film was placed between layers 3 and 4 (midplane) in the preform (before-cure) to create an initial delamination crack up to 75 mm from the clamped edges. A single pin was inserted in each sample a further 15 mm away from end of the initial delamination crack. Additional crack growth between 3 and 5 mm beyond the initial crack was first achieved by applying opening crosshead displacement at a rate of 5 mm/min. The crack length was observed and recorded from both sides of the specimen, ensuring that the difference was less than 2 mm. The crosshead was then brought back to 0 mm then displaced again at a rate of 1 mm/min. During the tests the applied load and crosshead displacement were recorded automatically, and the crack length was determined visually and recorded alongside the corresponding load and displacement regularly.

2.5. Optical microscopy

Specimens were machined to lengths around 25 mm with the pin at the centre and mounted in resin where specimens were placed in a pot and submerged in a 2-part resin-hardener mixture. An 8:1 ratio of EpoFix resin to hardener, manufactured by Struers, was used. The area of interest was then polished and observed under a Zeiss Leica Stemi 508 stereo microscope.

2.6. Mode I interlaminar finite element model

To further investigate the pre-pin load rise phenomena observed in

ø2.0 mm specimens in Section 3.3, the delamination response of a ø2.0 mm DCB specimen was modelled using the MSC.Marc [39] finite element solver. Geometry and dimensions are shown in Fig. 2. The DCB specimen was modelled as a 125 mm × 20 mm square made of two beams, one for the upper arm and one for the lower arm. Each arm comprised 3 layers of BX180-220- $[0/90F]_3$ - with a nominal thickness of 2 mm. Full integration hex continuum elements (MSC.Marc element type [40]) were used to model the upper and lower beams. The average size and distribution of the elements is given in Fig. 2. Composite material parameters are summarised in Table 2 and all layers were oriented in line with the orientation vectors – x = (1 0 0), y = (0 1 0), z = (0 0 1). The stainless-steel pin was modelled as a ø2.0 mm × 4 mm cylinder using full integration hex continuum elements (MSC.Marc element type [40]) for which material parameters are given in Table 2. An initial crack of 55 mm length and thickness 20 μm was placed between layers 3 and 4. The delamination region was modelled with full integration hex cohesive zone elements (MSC.Marc element type [40]) with thickness 20 μm which extended the end of the pre-crack to the end of the sample. Cohesive element parameters used for the analysis followed a linear model and are as follows: cohesive energy (G_{IC}) = 550 J/m^2 (taken from the average baseline G_{IC} in unpinned experimental results presented in Fig. 8), critical crack opening displacement = 2.5 × 10^{-5} m, maximum opening displacement = 1 × 10^{-4} m.

Touching contact in MSC.Marc notation (nonpenetration constraint that still allows relative sliding) was defined between the upper and lower laminate arms. A glued contact in MSC.Marc notation (supresses all relative motions between bodies through tying applying to at all degrees of freedom of nodes in contact, $u_{all\ relative} = 0$) was defined between the pin and the composite arms with an interference fit. A glue breaking transition to a touching contact condition between the pin and the laminate was defined with a normal stress threshold (σ) = 46 MPa which is the resin strength [31], and a tangential stress threshold (τ) = 23.2 MPa [42]. Upon breaking of the glued contact, the pin-laminate contact transitions to a touching type contact with a frictionless penalty. A boundary condition is applied to the bottom left edge nodes on the lower arm ($u_1 = u_2 = u_3 = u_{r1} = u_{r3} = 0$) and the nodes on the right face of the cantilever ($u_2 = u_{r1} = u_{r3} = 0$) and a displacement rate of 1 mm/min to a maximum displacement of 30 mm in the z-direction is applied to the nodes at the top right edge of the upper arm.

3. Results and discussion

3.1. Tension

Fig. 3 shows typical stress versus strain curves for unpinned and pinned specimens. Curves generally show good repeatability and a typical composite stress–strain response with a linear elastic region followed by brittle failure with no yielding. Fig. 4 compares the average tensile strength, modulus, and strain to failure of all specimen configurations. Tensile strength is generally unaffected by the presence of the pin up to ø2.0. The curves exhibit some pseudo-bilinear behaviour (likely resulting from the presence of ±45° plies) which becomes more pronounced as the pin diameter increases, tending to the unpinned behaviour. These have averaged transition points at 0.0023, 0.0027, 0.0029 and 0.0037 strain for the unpinned, ø1.2, ø1.5, and ø 2.0 specimens, respectively. Moduli are determined from the initial small strain (between 0 and 0.002) for consistency. Modulus doubles to its highest value, in going from unpinned to ø1.2 specimens. As the pin diameter increases, modulus decreases by 12 % from ø1.2 pins to ø1.5 pins, and by a further 14 % from ø1.5 pins to ø2.0 pins. The modulus in all pinned cases is still higher than in the unpinned case. Failure strain is significantly reduced by a maximum of 59 % from around 0.017 (±0.00082) in unpinned to 0.007 (±0.00093) strain in ø1.2 pinned materials.

Although the tensile failure strength of the material is unaffected, the way in which specimens fail is greatly influenced by the presence of the pin as shown in Fig. 5. Tensile failure transitions from large scale delamination dominated failure in unpinned specimens (Fig. 5a) to a combination of inter- and intra-laminar cracking in pinned specimens (Fig. 5b-d). This is accompanied by significant amounts of tow rupture and leads, in some cases (e.g., most ø1.2 mm specimens), to complete specimen fracturing. This extensive delamination type failure in unpinned specimens is typical of woven twill architectures where off-axis plies are included [43] and is the reason for the serrated region in the later stages of the unpinned load displacement graph (Fig. 3). Woven off-axis plies undergo scissoring during loading (Fig. 5a) in which yarns permanently rotate to align with the loading direction causing large shear strain in those plies [44]. It is the mismatch in the ability of the surface plies (0/90°) to strain alongside the interior plies (±45°) that causes the delamination and failure in unpinned specimens. The embedding of the pin therefore acts to partially suppress this delamination phenomenon, which is supported by an improvement in G_{IC} reported later in Section 3.3. This has the effect of significantly and expectedly reducing failure strain (Fig. 3) by constricting the amount of scissoring that can occur, but simultaneously encourages interfacial

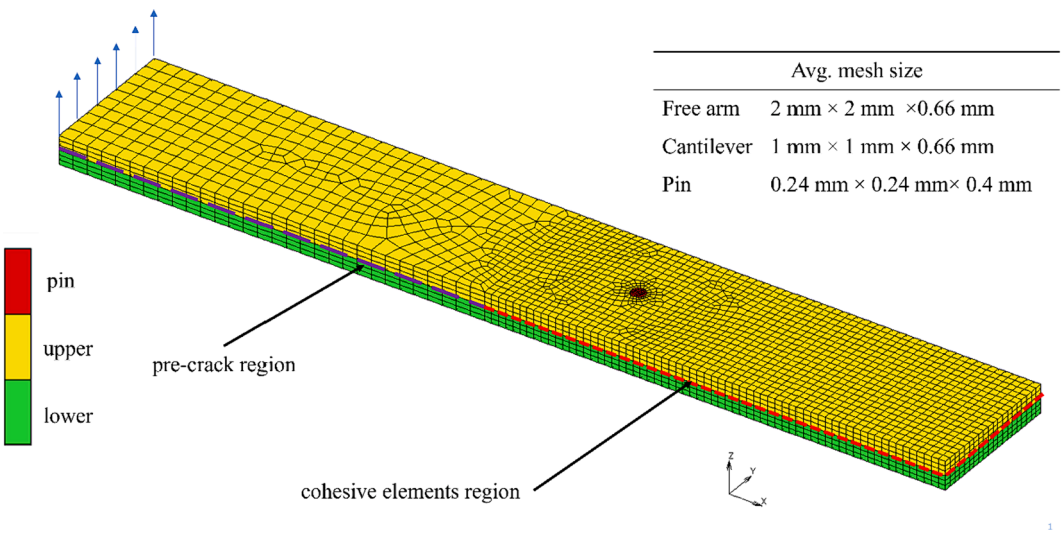

Fig. 2. Three-dimensional model of ø2.0 pinned DCB specimens showing geometry and mesh used for analysis.

Table 2
Laminate properties [41] and stainless-steel pins [33] used for pinned DCB analysis.

Material	E_1 (GPa)	E_2 (GPa)	E_3 (GPa)	ν_{12}	ν_{23}	ν_{31}	G_{12} (GPa)	G_{23} (GPa)	G_{31} (GPa)
Laminate	49.6	49.6	7.5	0.22	0.14	0.14	11.3	2.0	2.0
Pin	193*	–	–	0.275*	–	–	–	–	–

* Pin can be considered isotropic and therefore $E_1 = E$ and $\nu_{12} = \nu$ for used for pin material in FE simulation.

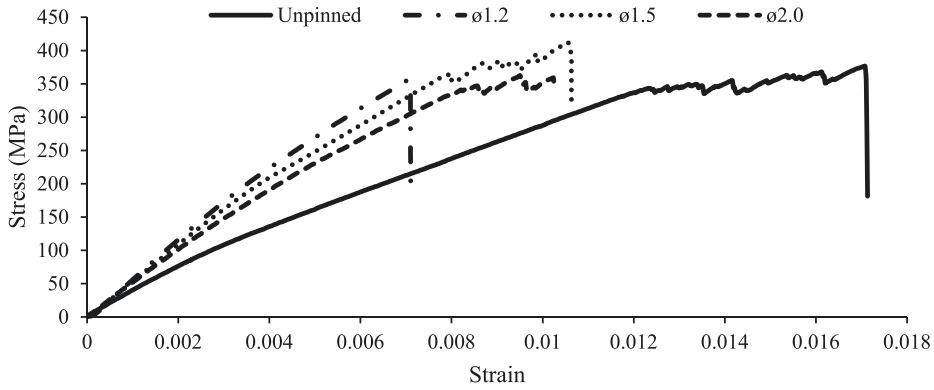

Fig. 3. Typical tensile stress versus strain curves for unpinned and pinned samples.

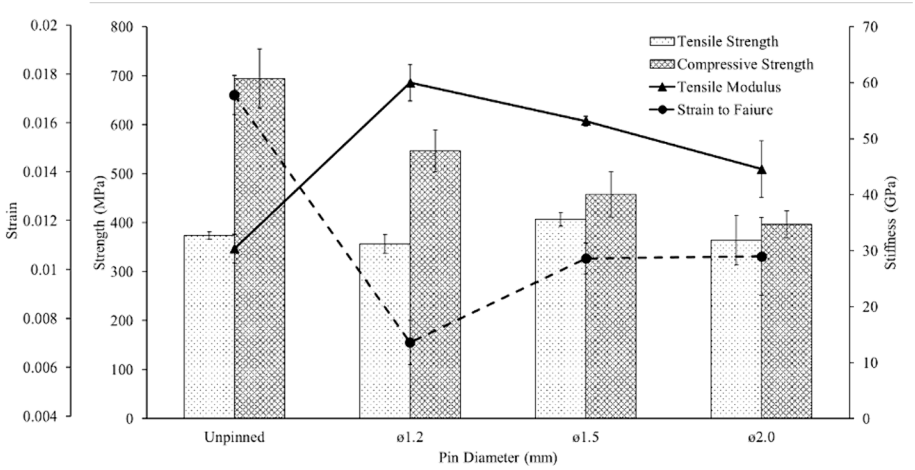

Fig. 4. Variation of tensile and compression properties of pinned and unpinned specimens with respect to pin diameter.

failure (fibre–matrix) and higher energy fibre-dominated failure in the form of tow rupture.

Failure in pinned specimens initiates at the pin-composite interface and propagates transverse to the loading direction along the cross-section. This failure progression is like what was observed in 3 to 9 mm diameter moulded-in holes in twill weave composites reported in [24], but is initially more progressive than catastrophic. In the case of the pinned specimens, it is the stiffness mismatch between the pin and laminate which leads to initial interfacial (pin-laminate) failure under deformation and subsequent laminate crack propagation from that initiation point. This is opposed to crack initiation at and propagation from the notched stress concentration in moulded-in open holes. In this case the advantages provided by change in the failure mode observed in pinned specimens seem to largely balance out expected reduction in tensile strength. Furthermore, the pin diameter does not influence the tensile strength in agreement with observations in moulded in holes where the size of the hole, between 6 and 10 mm in diameter, was reported not to affect tensile strength [19]. This can be explained based on the constant width to diameter across the different pin sizes and the expectation of similar stress concentration factors around a filled circular opening with the fibre orientation distributions also scaling around the pin.

Modulus is improved by the presence of the pin, doubling in 1.2 mm pinned samples. This is due to the restraining of the scissoring effect in ±45° plies in which bias extension is a shear dominated event. Modulus is very sensitive to the presence of the ±45° plies because of this bias extension effect [47]. The pin is locked within in a unit cell, and because of the woven nature of the layers, local restraining of bias extension is limited within a unit cell. Increasing pin diameter increases the specimen width in accordance with the testing standard ($w/d_{pin} = 6$) and so increases the number of unaffected tows along the cross section which results in the modulus tending towards the unpinned value.

The literature surrounding this type of experimental fracture mechanics evaluation for similar processes is extremely limited. Very similar findings were reported for both strength and modulus when evaluating 4 mm diameter brass filled moulded-in (filled and open-hole) holes in woven jute-epoxy/-polyester composites [17]. A slight improvement was observed in tensile strength and a significant improvement in modulus at the expense of failure strain, supporting the findings of this study. This result was attributed to an increase in load

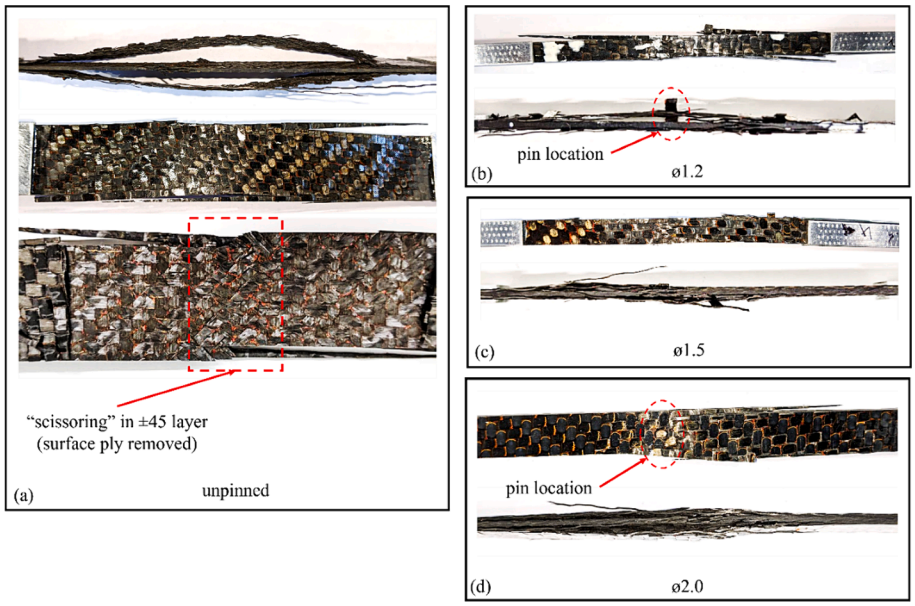

Fig. 5. Fractured tensile specimens showing (a) unpinned, (b) ø1.2, (c) ø1.5, and (d) ø2.0.

bearing capacity around the hole because of a localised increase in volume fraction (v_f) from the unbroken deviated tows. These findings are supported by a series of works which also report no deterioration in tensile strength in similarly sized (and even much larger) moulded in holes (open-hole) in woven composites due to preservation of tow integrity and increased v_f around the hole [19,24].

3.2. Compression

Fig. 4 compares average compressive strength across all configurations. Unlike tensile strength, compressive strength is greatly reduced by the presence of the pin in the laminate. Strength reduces by 22 % from unpinned to ø1.2 samples, a further 34 % from ø1.2 to ø1.5 and a further 29 % from ø1.5 to ø2.0 samples.

Like tensile specimens, significant differences are noted in the compressive failure mechanisms present in unpinned and pinned specimens. Fig. 6 shows micrographs that compare the failure mechanisms in unpinned and pinned samples. The perceived taper of the pin is due to the slightly angled cutting plane of the micrographs. Failure in unpinned samples is transverse through-thickness shear failure (Fig. 6a) which is a high-energy, fibre-dominated failure mode in composites and supports the high compression strength value. Compression failure in woven composites is usually a combination of local microstructural, kink band, interlaminar and intralaminar failures that coalesce to a macrostructural failure event [21,45–47]. In the case of the transverse shear failure evident in Fig. 6, this is typically the result of local kink band formation in loading aligned tows and interfacial failures in non-aligned tows that merge following shear planes arising from the crimp and waviness regions in the woven architecture. Pinned specimens instead show signs of local inter- and intra-ply delamination both in the region near (Fig. 6b and c) and away from the pin (Fig. 6d). Crushing either side of the pin is also observed in the micrographs of the larger ø2.0 mm pin samples (Fig. 6c). Intralaminar cracking is visible in the region directly around the pin and extends outwards, becoming more pronounced where the

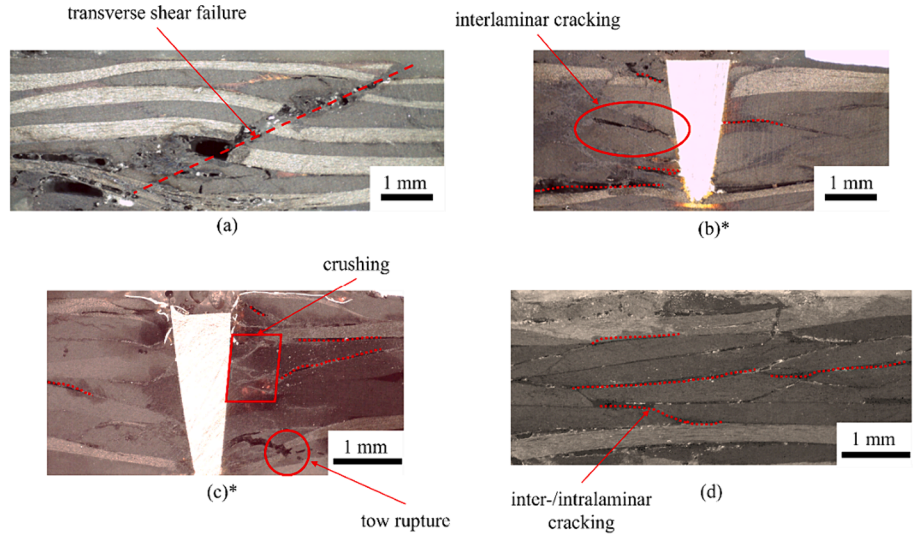

*note that the perceived taper of the pins is due to the cutting plane.

Fig. 6. Micrographs showing compressive failure mechanics in (a) unpinned, (b) pin location in ø1.2, (c) pin location in ø2.0, and (d) away from the pin in ø2.0 specimens.

effects of local pin delamination resistance are not apparent. This represents a transition from higher-energy, fibre-dominated failure in unpinned samples to lower-energy matrix dominated failure in pinned samples and is responsible for the significant deterioration in compressive strength.

Compressive strength in composites is extremely sensitive to crimp and waviness. As pin diameter increases, local fibre crimp and waviness in the region immediately surrounding the pin increase. Although the static insertion method seems to do a good job of minimising this effect [12], both local tow disturbance and local v_f variations inevitably increase non-linearly with pin diameter. This added waviness promotes interlaminar failures that shows signs of delamination buckling failure and subsequent splaying. This is typical of woven architectures and is a consequence of the bending forces on yarns [45] which, in this case, is exacerbated by heavily deviated yarn paths at the pin.

3.3. Mode I interlaminar

In DCB testing, during loading all specimens showed a symmetric response with no twisting whilst the crack front position appeared uniform across the two faces of the specimen. The load–displacement curves are shown in Fig. 7 and are shown as a means of validating the FE model. In unpinned specimens, crack initiation occurs at around 40 N (±4N) followed by a gradual decrease to steady state crack propagation. In pinned samples, this load is delayed and increased as the crack is arrested by the pin, after which a load decrease is observed. The load–displacement data is applied using the corrected beam theory (CBT) method for deriving G_{IC}, which is detailed in the ISO 15024 standard [38], and used to derive the interlaminar toughness curves using Eq. (1). Experimentally calculated G_{IC} values are shown in Fig. 8.

$$G_{IC} = \frac{3P\delta}{2b(a+|\Delta|)} \times \frac{F}{N} \tag{1}$$

Where P is the load, δ is the load displacement, a is delamination length, b is the specimen width, C is the load line compliance (δ/P), Δ is the x-intercept of a graph of delamination length (a) versus $(C/N)^{1/3}$, F is the large-displacement correction (described below in Eq. (2)), N is the load block correction (described below in Eq. (3)),

$$F = 1 - \frac{3}{10}\left(\frac{\delta}{a}\right)^2 - \frac{2}{3}\left(\frac{\delta l_1}{a^2}\right) \tag{2}$$

$$N = 1 - \left(\frac{l_2}{a}\right)^3 - \frac{9}{8}\left[1 - \left(\frac{l_2}{a}\right)^2\right]\frac{\delta l_1}{a^2} - \frac{9}{35}\left(\frac{\delta}{a}\right)^2 \tag{3}$$

Where a is δ is the load displacement, a is delamination length, l_1 is the distance from the centre of the loading pin to the midplane of the specimen beam and l_2 is the distance from the loading-pin centre to its edge.

Fig. 8 compares averaged crack resistance curves for unpinned and pinned specimens. Crack growth is stable and follows a stick–slip propagation; however, a large ~10 mm jump is observed as the crack front approaches the pin, hence the high variation in fracture toughness results. Unpinned specimens show an average crack energy release rate of 550 J/m^2 (±21 J/m^2) for the duration of the delamination event. In pinned samples, there is a linear increase to a peak around the location of the pin. The average peak crack energy release rates observed during bridging are 854 J/m^2 (±191 J/m^2) in ø1.2 specimens, 1018 J/m^2 (±287 J/m^2) in ø1.5 specimens and 931 J/m^2 (±251 J/m^2) in ø2.0 specimens. After the end of bridging, G_{IC} reduces back to levels similar to the baseline of the unpinned specimens. There is clearly an improvement in G_{IC} due to the presence of the pin but given the large standard deviation in the results likely resulting from unstable crack propagation at the pin. There is no significant relationship between delamination resistance and pin diameter.

The failure progression in pinned samples is shown in Fig. 9. In all pinned cases the delamination crack progresses towards the pin and on reaching the vicinity of the pin there is a sharp rise in load (Fig. 7). Typically, this increase would come at or after the reinforcement point as bridging traction kicks in. However, unlike in tufting or stitching, there is no need for straightening of the through-thickness reinforcement before this effect is apparent as interfacial failure between the pin and the laminate is likely before the pin deforms significantly under bridging tension. This is not the case for ø2.0 specimens where the peak load is achieved well ahead of the crack reaching the pin. The general trend observed is that the peak load moves forward as the pin diameter increases. There is an audible general debonding at the interface between the pin and the composite followed by pin pull-out. Because the strength of the pin is an order of magnitude higher than that of the matrix-pin bond [33,42] the pin does not break, instead only pulls out and resists crack opening via friction between the pin and the hole left behind (Fig. 9b).

The finite element model of DCB testing was used to investigate the reasons behind the early onset delamination performance improvement in ø2.0 specimens. Fig. 7 compares the load versus opening displacement results of the simulation with the experiment and shows a generally good agreement between the two. Fig. 10 shows the stress distribution at the delamination interface when the crack is 5 mm before the pin. Although the crack is in front of the pin, there is already a significant bending stress developed in the pin which is transferred from the bending of the cantilever arms as the crack is opened which corresponds with the increase in load. This earlier onset in G_{IC} is only effective in this way when pin diameters are large. In tufted and z-pinned laminates where reinforcement allows sufficient yielding (metallic

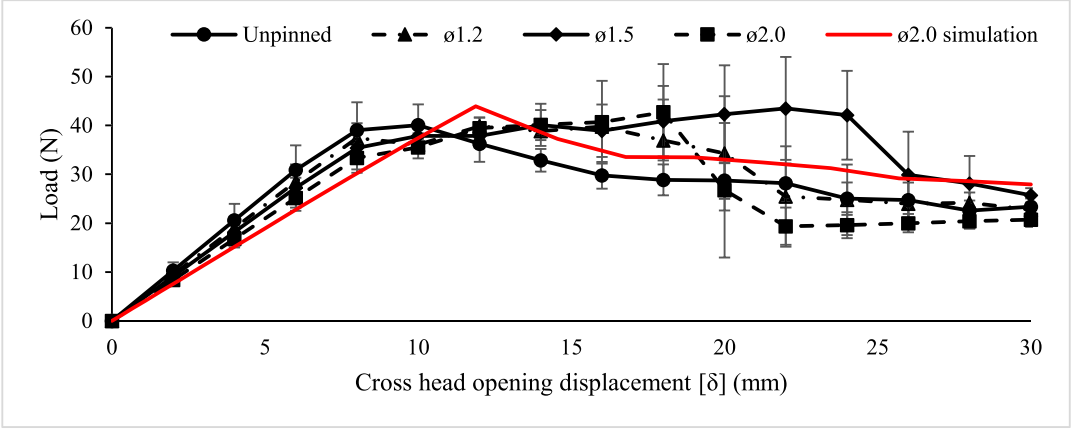

Fig. 7. Averaged load displacement curves for unpinned and pinned laminates.

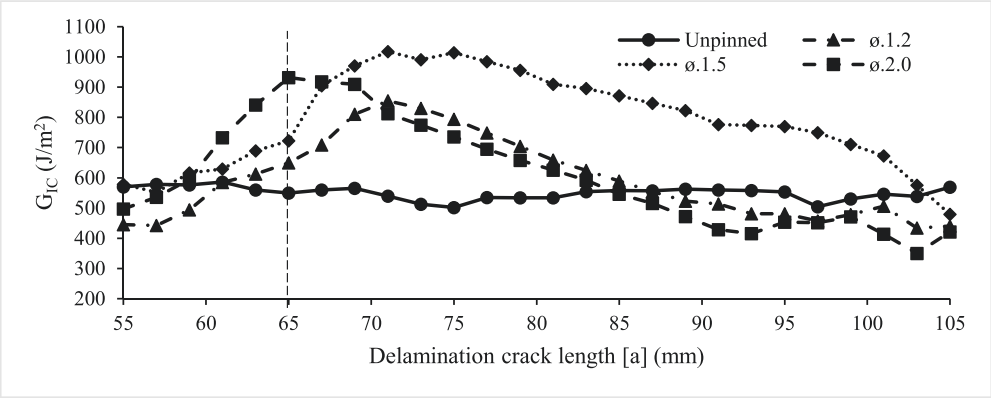

Fig. 8. Averaged delamination fracture toughness versus crack length for unpinned and pinned laminates; pin located at a = 65 mm.

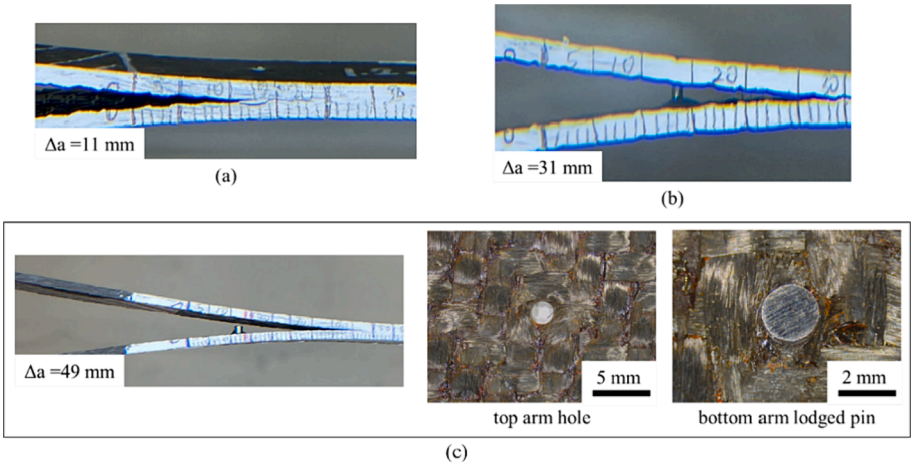

Fig. 9. Typical delamination crack progression (a) at the pin (Δa = 11 mm), (b) just after the pin (Δa = 31 mm), (c) long after the pin (Δa = 49 mm).

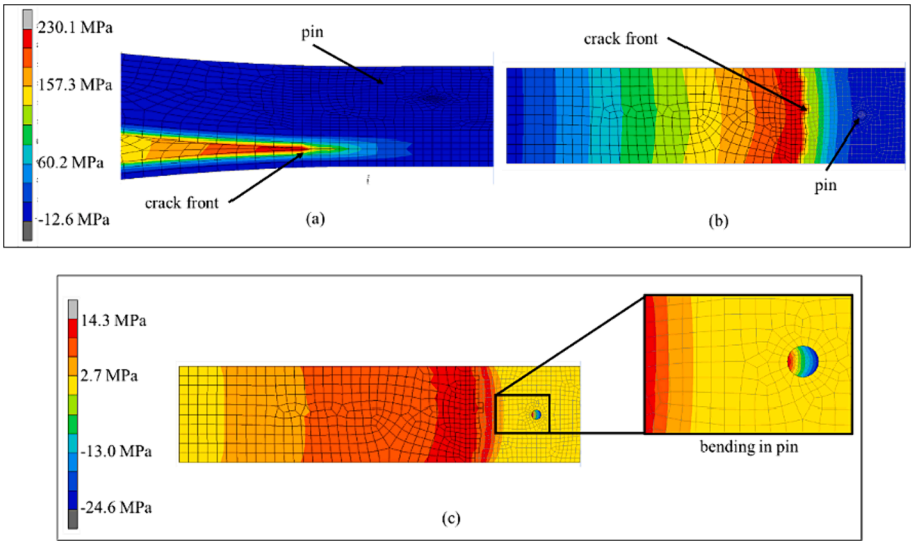

Fig. 10. Stress contour plots for crack extension at 5 mm ahead of the pin (Δa = 5 mm) showing (a) maximum principal stress at crack, (b) maximum principal stress at the delamination plane, and (c) 33 component of stress at the pin.

reinforcements), this similarly results in bending stresses being maintained by the reinforcements during DCB tests [48].

The pull out of the large diameter metallic pin that occurs during mode I delamination is like what occurs locally at the pin in metallic z-pinned laminates with some notable differences. Because of the much greater pin stiffness due to the large cross-sectional areas, plastic deformation of the pin is not likely. Snubbing, which is the lateral deflection of the pin large due to crack sliding displacements, is still

possible after debonding and is likely dependent on the length to diameter ratio of the pin. This has the effect of increasing friction between the pin and the laminate and increases resistance against shear induced pull-out. Numerical modelling of the snubbing mechanism has concluded that in conjunction with increasing the bridging force, it also increases the energy dissipation [49]. The pull-out response of a single pin can be characterised by a tri-linear curve and can be divided into two subcategories: (a) instant debonding and (b) gradual debonding [50]. Fig. 7 suggests that the debonding in ø2.0 mm samples is gradual over a small time period, with a linear drop in force over an increase in displacement. This occurs when the pin does not de-bond instantly but over a period of time, during which energy is consumed both by debonding and frictional sliding. After complete interfacial debonding, the only mechanism that works is frictional sliding until the pin is completely pulled-out of the laminate.

4. Conclusion

This work characterised the effect of single pin insertion using the static insertion method on the mechanical behaviour and associated fracture mechanics of woven carbon-benzoxazine composites with large a single diameter metallic pin inserted using the static pin insertion method. Pin diameters ranged from 1.2 to 2.0 mm in diameter and pinned laminates were investigated under tension, compression, and mode I delamination loading conditions.

Tensile strength was found to be unaffected by the presence of the pin in laminates. The addition of the pin altered the macroscale fracture mechanics of the laminate from matrix-dominated delamination in unpinned laminates to fibre-dominated tow rupture in pinned samples. This effective suppression of delamination had the effect of maintaining the tensile strength in the material by altering the failure mechanisms. Tensile modulus was significantly improved in pinned laminates by up to 100 % in 1.2 mm diameter pin specimens.

Compression response was markedly affected by the insertion of the pin. Compressive strength decreased by a maximum of 42 % in 2.0 mm diameter pinned laminates. The decrease in compressive strength was attributed to a severe increase in local crimp and waviness at the pin, which serves as an initiation point for premature failure in the material. Compression strength decreases with increasing pin diameter which is responsible for increasing local tow waviness. This results in a transition from high-energy transverse shear failure in unpinned laminates to interlaminar failure via delamination buckling in pinned laminates.

There is an increase in peak average G_{IC} values at the pin in pinned laminates by a maximum of 86 %. There is no statistically significant trend in the relationship peak G_{IC} and pin diameter. A new observation here is that the initial increase in the slope of the G_{IC} curve and the location of the peak value shift forwards with increasing pin diameter. In 2.0 mm diameter pinned laminates, the initial rise in G_{IC} is observed in front of the crack reaching the pin and the peak is at pin itself, which is unlike the conventional crack bridging understanding where the G_{IC} rise is observed at or after the pin. This was found to be the result of pin bending which initiates before the delamination crack reaches the pin.

This work has demonstrated that the insertion of a large diameter pin, far exceeding the capabilities of current TTR methods, is also compatible with structural composites as far as tensile and through-thickness performance are required. This result is significant insofar as proving that through-thickness reinforcing elements of this magnitude can be inserted in this way, without significant diminishment in structural performance (excluding in compression) local to the pin with potential for integrating fluid flow channels, joining, or functional reinforcements like heating elements. The interpretation of these results is limited to the use of a fairly rigid and ductile pin material and investigations into non-symmetric loading configurations or the collective effect of pins in arrays are still needed. The improvements in mode I delamination resistance can positively affect laminates but are not sufficient to provide large scale local performance improvements. This reinforces the notion that the static insertion technology can be applied to the integration of large diameter multifunctional elements, joining applications, and the more efficient integration of moulded-in holes without having adverse effects on part quality or performance. The results here can be expanded to inform a future study where similar large diameter pins arranged as an array to investigate the collective effective multiple pins in the structure on both structural and functional performance.

CRediT authorship contribution statement

Geoffrey Neale: Conceptualization, Data curation, Formal analysis, Investigation, Methodology, Project administration, Resources, Supervision, Validation, Visualization, Writing – original draft, Writing – review & editing. **Vinodhen Saaran:** Data curation, Formal analysis, Investigation, Methodology, Writing – original draft. **Monali Dahale:** Data curation, Formal analysis. **Alex Skordos:** Conceptualization, Formal analysis, Funding acquisition, Methodology, Project administration, Supervision, Visualization, Writing – review & editing.

Data availability

Data underlying this study can be accessed through the Cranfield University repository at [51].

Declaration of competing interest

The authors declare the following financial interests/personal relationships which may be considered as potential competing interests: Geoffrey Neale reports financial support was provided by Horizon 2020.

Acknowledgements

This work was supported by the SEER project which has received funding from the European Union's Horizon 2020 research and innovation programme (Grant agreement 871875).

References

[1] Koumoulos E, Trompeta A-F, Santos R-M, Martins M, Santos C, Iglesias V, et al. Research and development in carbon fibers and advanced high-performance composites supply chain in Europe: a roadmap for challenges and the industrial uptake. J Compos Sci 2019;3:86. https://doi.org/10.3390/jcs3030086.
[2] Partridge IK, Cartié DDR. Delamination resistant laminates by Z-fiber® pinning: Part I manufacture and fracture performance. Compos Part A Appl Sci Manuf 2005;36:55–64. https://doi.org/10.1016/j.compositesa.2004.06.029.
[3] Dransfield KA, Jain LK, Mai YW. On the effects of stitching in CFRPs—I. mode I delamination toughness. Compos Sci Technol 1998;58:815–27. https://doi.org/10.1016/S0266-3538(97)00229-7.
[4] Grigoriou K, Ladani RB, Mouritz AP. Electrical properties of multifunctional Z-pinned sandwich composites. Compos Sci Technol 2019;170:60–9. https://doi.org/10.1016/j.compscitech.2018.11.030.
[5] Pegorin F, Pingkarawat K, Mouritz AP. Controlling the electrical conductivity of fibre-polymer composites using z-pins. Compos Sci Technol 2017;150:167–73. https://doi.org/10.1016/j.compscitech.2017.07.018.
[6] O'Keeffe C, Pickard LR, Cao J, Allegri G, Partridge IK, Ivanov DS. Multi-material braids for multifunctional laminates: conductive through-thickness reinforcement. Funct Compos Mater 2021;2. https://doi.org/10.1186/s42252-021-00018-0.
[7] Lombetti DM, Skordos AA. Lightning strike and delamination performance of metal tufted carbon composites. Compos Struct 2019;209:694–9. https://doi.org/10.1016/j.compstruct.2018.11.005.
[8] Zhang B, Allegri G, Hallett SR. An experimental investigation into multi-functional Z-pinned composite laminates. Mater Des 2016;108:679–88. https://doi.org/10.1016/j.matdes.2016.07.035.
[9] Koh TM, Feih S, Mouritz AP. Experimental determination of the structural properties and strengthening mechanisms of z-pinned composite T-joints. Compos Struct 2011;93:2222–30. https://doi.org/10.1016/j.compstruct.2011.03.009.
[10] Löbel T, Kolesnikov B, Scheffler S, Stahl A, Hühne C. Enhanced tensile strength of composite joints by using staple-like pins: working principles and experimental validation. Compos Struct 2013;106:453–60. https://doi.org/10.1016/J.COMPSTRUCT.2013.06.020.
[11] Arnautov A, Nasibullins A, Gribniak V, Blumbergs I, Hauka M. Experimental characterization of the properties of double-lap needled and hybrid joints of

carbon/epoxy composites. Materials 2015;8:7578–86. https://doi.org/10.3390/ma8115410.
[12] Neale G, Skordos A. Insertion of large diameter through-thickness metallic pins in composites. Mater Des 2022;216:110559. https://doi.org/10.1016/j.matdes.2022.110559.
[13] Galińska A. Mechanical joining of fibre reinforced Polymer composites to metals—A review Part I: Bolted Joining. Polymers (Basel) 2020;12:2252. https://doi.org/10.3390/polym12102252.
[14] Gnaba I, Legrand X, Wang P, Soulat D. Through-the-thickness reinforcement for composite structures: a review. J Ind Text 2019;49:71–96. https://doi.org/10.1177/1528083718772299.
[15] Kostopoulos V, Sarantinos N, Tsantzalis S. Review of through-the-thickness reinforced z-pinned composites. J Compos Sci 2020;4:31. https://doi.org/10.3390/jcs4010031.
[16] Zervos C, Poulopoulos G, Missinne J, Szaj M, Avramopoulos H. Miniaturized silicon photonics multi-sensor operating at high temperatures for use in composite materials industrial applications. In: Busse LE, editor. Photonic Instrumentation Engineering IX, San Francisco: 2022. doi: 10.1117/12.2606053.
[17] Kumar J, Singh I. Comparative analysis of molded and drilled holes in jute fiber reinforced plastic laminates. J Nat Fibers 2022;19:7363–73. https://doi.org/10.1080/15440478.2021.1946880.
[18] Zitoune R, Crouzeix L, Collombet F, Tamine T, Grunevald Y-H. Behaviour of composite plates with drilled and moulded hole under tensile load. Compos Struct 2011;93:2384–91. https://doi.org/10.1016/j.compstruct.2011.03.027.
[19] Langella A, Durante M. Comparison of tensile strength of composite material elements with drilled and molded-in holes. Appl Compos Mater 2008;15:227–39. https://doi.org/10.1007/s10443-008-9069-z.
[20] Hufenbach W, Gottwald R, Kupfer R. Bolted Joints With Moulded Holes For Textile Thermoplastic Composites. 2011.
[21] Gutkin R, Pinho ST. Combining damage and friction to model compressive damage growth in fibre-reinforced composites. J Compos Mater 2015;49:2483–95. https://doi.org/10.1177/0021998314549614.
[22] Mouritz AP. Compression properties of z-pinned composite laminates. Compos Sci Technol 2007;67:3110–20. https://doi.org/10.1016/j.compscitech.2007.04.017.
[23] Özaslan E, Yetgin A, Acar B. Stress concentration and strength prediction of 2×2 twill weave fabric composite with a circular hole. J Compos Mater 2019;53:463–74. https://doi.org/10.1177/0021998318785994.
[24] Ng SP, Tse PC, Lau KJ. Progressive failure analysis of 2/2 twill weave fabric composites with moulded-in circular hole. Compos B Eng 2001;32:139–52. https://doi.org/10.1016/S1359-8368(00)00040-8.
[25] Chang LW, Yau SS, Chou TW. Notched strength of woven fabric composites with moulded-in holes. Composites 1987;18:233–41. https://doi.org/10.1016/0010-4361(87)90413-7.
[26] Ghasemi Nejhad MN, Chou TW. Compression behaviour of woven carbon fibre-reinforced epoxy composites with moulded-in and drilled holes. Composites 1990;21:33–40. https://doi.org/10.1016/0010-4361(90)90096-F.
[27] Sawicki AJ, Minguet PJ. Failure mechanisms in compression-loaded composite laminates containing open and filled holes. J Reinf Plast Compos 1999;18:1708–28. https://doi.org/10.1177/073168449901801805.
[28] Bianchi F, Zhang X. A cohesive zone model for predicting delamination suppression in z-pinned laminates. Compos Sci Technol 2011;71:1898–907. https://doi.org/10.1016/j.compscitech.2011.09.004.
[29] Cui H, Li Y, Koussios S, Beukers A. Mixed mode cohesive law for Z-pinned composite analyses. Comput Mater Sci 2013;75:60–8. https://doi.org/10.1016/j.commatsci.2013.04.006.
[30] Rugg KL, Cox BN, Ward KE, Sherrick GO. Damage mechanisms for angled through-thickness rod reinforcement in carbon-epoxy laminates. Compos Part A Appl Sci Manuf 1998;29:1603–13. https://doi.org/10.1016/S1359-835X(98)00087-6.
[31] SHD Composites. BX180-220 Benzoxazine Tooling Prepreg - Product Datasheet 2017.
[32] Rimdusit S, Jubsilp C, Tiptipakorn S. Introduction to Commercial benzoxazine and their unique properties. In: Alloys and Composites of Polybenzoxazines, Engineering Materials. Singapore: Springer Science+Business Media; 2013. p. 1–27. https://doi.org/10.1007/978-981-4451-76-5_1.
[33] Masteel UK Ltd. Grade 304H Stainless Steel (UNS S30409) 2019. https://www.azom.com/article.aspx?ArticleID=5050 (accessed July 8, 2021).
[34] Stable Micro Systems. TA.HDplus Texture Analyser | Stable Micro Systems Products n.d. https://www.stablemicrosystems.com/TAHDplus.html (accessed August 24, 2021).
[35] ASTM. D3039/D3039M: Standard Test Method for Tensile Properties of Polymer Matrix Composite Materials. 2017. doi: 10.1520/D3039_D3039M-17.
[36] ASTM. D6742/D6742M − 17: Standard Practice for Filled-Hole Tension and Compression Testing of Polymer Matrix Composite Laminates. 2015. doi: 10.1520/D6742_D6742M-17.
[37] ASTM. D695−15: Standard Test Method for Compressive Properties of Rigid Plastics. 2015. doi: 10.1520/D0695-15.
[38] British Standard Organization. ISO 15024:2001 : Fibre-reinforced plastic composites : Determination of mode I interlaminar fracture toughness, GIC, for unidirectionally reinforced materials. ISO; 2001.
[39] MSC Software. Marc - Advanced Nonlinear Simulation Solution n.d. https://www.mscsoftware.com/product/marc (accessed July 8, 2021).
[40] Marc® 2019 - Volume B: Element Library 2019. https://hexagon.com/.
[41] Scida D, Aboura Z, Benzeggagh ML, Bocherens E. Prediction of the elastic behaviour of hybrid and non-hybrid woven composites. Compos Sci Technol 1998;57:1727–40. https://doi.org/10.1016/S0266-3538(97)00105-X.
[42] Li H, Qu C, Wang D, Liu C. Adhesive of Benzoxazine Resin and Adhesion Property. International Conference on Composite Materials (ICCM21), Xi'an: 2017.
[43] Zhou G, Sun Q, Li D, Meng Z, Peng Y, Zeng D, et al. Effects of fabric architectures on mechanical and damage behaviors in carbon/epoxy woven composites under multiaxial stress states. Polym Test 2020:90. https://doi.org/10.1016/j.polymertesting.2020.106657.
[44] Koohbor B, Ravindran S, Kidane A. Meso-scale strain localization and failure response of an orthotropic woven glass-fiber reinforced composite. Compos B Eng 2015;78:308–18. https://doi.org/10.1016/j.compositesb.2015.03.064.
[45] Opelt CV, Cândido GM, Rezende MC. Compressive failure of fiber reinforced polymer composites – a fractographic study of the compression failure modes. Mater Today Commun 2018;15:218–27. https://doi.org/10.1016/j.mtcomm.2018.03.012.
[46] De Carvalho NV, Pinho ST, Robinson P. An experimental study of failure initiation and propagation in 2D woven composites under compression. Compos Sci Technol 2011;71:1316–25. https://doi.org/10.1016/j.compscitech.2011.04.019.
[47] Wilkinson E, Parry TV, Wronski AS. Compressive failure in two types of carbon fibre-epoxide laminates. Compos Sci Technol 1986;26:17–29. https://doi.org/10.1016/0266-3538(86)90053-9.
[48] M'membe B, Yasaee M, Hallett SR, Partridge IK. Effective use of metallic Z-pins for composites' through-thickness reinforcement. Compos Sci Technol 2019;175:77–84. https://doi.org/10.1016/j.compscitech.2019.02.024.
[49] Cartié DDR, Cox BN, Fleck NA. Mechanisms of crack bridging by composite and metallic rods. Compos Part A Appl Sci Manuf 2004;35:1325–36. https://doi.org/10.1016/j.compositesa.2004.03.006.
[50] Gornet L, Ijaz H, Cartié DDR. Inelastic interface damage modeling with friction effects: application to Z-pinning reinforcement in carbon fiber epoxy matrix laminates. J Compos Mater 2010;44:2067–81. https://doi.org/10.1177/0021998309359214.
[51] Neale G, Saaran V, Dahale M, Skordos A. An evaluation of large diameter through-thickness metallic pins in composites: dataset. Cranfield Online Research Data Repository 2022. https://doi.org/10.17862/cranfield.rd.21259122.

2024-03-24

An evaluation of large diameter through-thickness metallic pins in composites

Neale, Geoffrey

Elsevier

Neale G, Saaran V, Dahale M, Skordos AA. (2024) An evaluation of large diameter through-thickness metallic pins in composites, Composite Structures, Volume 337, June 2024, Article Number 118066

https://doi.org/10.1016/j.compstruct.2024.118066